Journal of Alloys and Compounds 507 (2010) 184–189

Contents lists available at ScienceDirect

Journal of Alloys and Compounds

journal homepage: www.elsevier.com/locate/jallcom

Electrical characterization and device characterization of ZnO microring shaped films by sol–gel method

Fahrettin Yakuphanoglu*

Firat University, Physics Department, Faculty of Science and Arts, 23119, Elazig, Turkey

ARTICLE INFO

Article history:
Received 30 March 2010
Received in revised form 20 July 2010
Accepted 21 July 2010
Available online 1 August 2010

Keywords:
ZnO
Sol–gel
Nanoparticles
Schottky diode

ABSTRACT

Zinc oxide microrings formed nanoparticles were prepared on n-type silicon substrate by sol–gel method. The structure of ZnO film is confirmed by XRD analysis and ZnO film exhibits a polycrystalline grown with a hexagonal wurtzite-type. The optical band gap of the ZnO film deposited on silicon substrate was determined using the reflectance spectra by means of Kubelka-Munk formula and was found to be 3.22 eV. The structural properties of the ZnO film were investigated by atomic force microscopy. The AFM results indicate that the ZnO film is consisted of microrings with nanoparticles. A single phase of ZnO microring with outer diameter is ranging from 2.2 μm to 1.72 μm and inner diameters ranging from 125 nm to 470 nm was obtained. A Schottky diode having Au/n-type ZnO plus n-type silicon structure was fabricated. The current–voltage and impedance spectroscopy properties of the diode have been investigated. The barrier height ϕ_b and ideality factor n values for the diode were found to be 0.80 eV and 2.01, respectively. The series resistance for the diode was calculated from the admittance behavior in accumulation region. The interface state density profile for the diode was obtained. The obtained results indicate that the electric parameters of the diode are affected by structural properties of ZnO film.

1. Introduction

Transparent conducting oxides (TCO) are of great interest in electronic and electro-optical applications and they are used in a variety of devices such as flat screens, thin film photovoltaic cells, dye-sensitized solar cells and light-emitting diodes (LEDs) [1–3]. Zinc oxide (ZnO), which is a wide band gap semiconductor [4], has attracted a great deal of interest because of many current and potential applications [5–9]. The device application of ZnO semiconductor plays an important role on investigation of the metal–semiconductor contacts. The performance of UV photodetectors based ZnO can be improved with a large Schottky barrier height, because, a large barrier height will lead to small leakage current and high breakdown voltage, and will improve the photoresponsivity and the photocurrent to dark current contrast ratio [10]. There are many works on ZnO Schottky diodes to improve their device performances [11–15].

On the other hand, nanoscale structures have attracted extensive synthetic attention as a result of their novel size-dependent properties [3,16,17]. Much attention has been focused on the research of nanostructure semiconductor materials due to their novel physical and chemical properties and wide range of potential applications in nanodevices [18]. Many useful methods have been used to prepare high quality ZnO thin films, such as, magnetron sputtering, metal-organic chemical vapor deposition (MOCVD), pulsed-laser deposition (PLD), molecular beam epitaxy (MBE) and sol–gel process [19–21]. Among these methods, the sol–gel method has some advantages to prepare large area ZnO thin films at low cost and easy technology [7] and also, sol–gel dip coating is a simple apparatus with low cost and it can be suitable for preparation of nanostructure ZnO films for electronic device applications [22]. With this connection, it is aimed to prepare the nanostructure ZnO film to fabricate a Schottky diode based on ZnO, because the performance of a Schottky diode is drastically influenced by physical properties of ZnO semiconductor used in junction.

To date, there has been very limited report on Schottky contacts of Au/n-ZnO/n-Si, especially for that of sol–gel ZnO thin films.

In present study, Zinc oxide microrings formed nanoparticles were synthesized by sol–gel method and an Au/n-ZnO/n-Si junction was fabricated. Some physical properties of ZnO and device performance of the Au/n-ZnO/n-Si diode have been investigated.

2. Experimental

The zinc oxide film was synthesized by sol–gel method. The used materials are zinc acetate hexahydrate as the starting material, deionized water as the solvent, and monoethanolamine as stabilizer. Equal concentrations of monoethanoamine and Zn^{2+} were used. The precursor solution was mixed with a magnetic stirrer for 2 h in 60 °C and then placed in air for 24 h resulting in a clear and homogeneous sol. The acid sol (pH 1) was prepared by adding nitric acid (HNO_3).

* Tel.: +90 424 2370000x3621; fax: +90 424 2330062.
E-mail addresses: fyhan@hotmail.com, fyahnoglu@firat.edu.tr.

0925-8388/$ – see front matter © 2010 Elsevier B.V. All rights reserved.
doi:10.1016/j.jallcom.2010.07.151

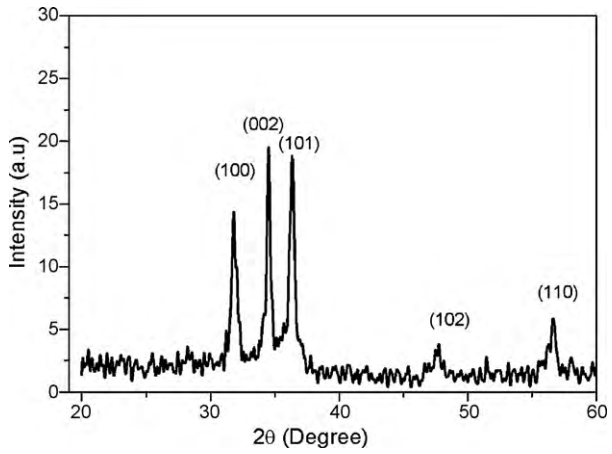

Fig. 1. X-ray diffraction spectra of the ZnO film.

For fabrication of the diode, n-type single crystal silicon substrate (600 μm thickness and 5–10 Ω cm) was used. The n-Si substrate was etched by HF and then was rinsed in deionised water using an ultrasonic bath for 10–15 min and finally was chemically cleaned according to method based on successive baths of methanol and acetone. Immediately after surface cleaning, an ohmic contact was prepared with high purity silver (Ag) metal (99.999%) with a thickness of 200 nm thermally evaporated onto the whole back surface of the wafer at the pressure of 4.5×10^{-5} Torr. Ohmicity of the contact was controlled by current–voltage measurements and the contact shows a good ohmic behavior. The film of ZnO was prepared on n-type silicon with ohmic contact by drop coating. For this, 40 μl of ZnO solution was dropped on front surface of the n-Si silicon substrate and ZnO/n-Si structure was stood on a hot plate at 150 °C for 2 h for evaporating the solvent. After a thin solid film on the substrate was formed, the film was annealed at 600 °C in a furnace at air atmosphere. The film thickness of ZnO was measured about 1 μm. An Au Schottky contact of 100 nm thickness was formed on ZnO film deposited on n-type silicon by VAKSIS thermal evaporation system under 4.5×10^{-5} Torr. The contact area of the diode was found to be 3.14×10^{-2} cm^2.

The reflectance spectra of the ZnO film on deposited n-type silicon were performed using a Shimadzu UV-VIS-NIR 3600 spectrophotometer using an integrating sphere attachment. The structural properties of the film were investigated by Park System XE-100E atomic force microscopy (AFM). The current–voltage and capacitance–conductance–voltage–frequency measurements were done using KEITHLEY 4200 semiconductor characterization system. X-ray diffraction (XRD) measurement was done by BRUKER D8 diffractometer.

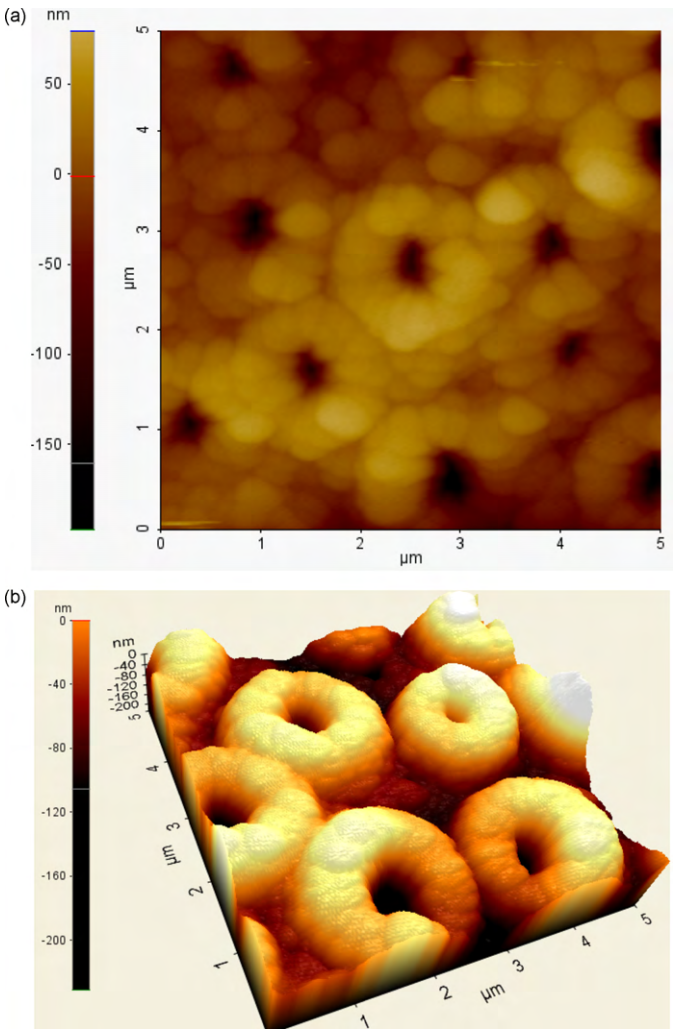

Fig. 2. AFM images of the ZnO film: (a) 1D; (b) 3D.

3. Results and discussion

3.1. Structural properties of the ZnO film

XRD spectra of the ZnO film are shown in Fig. 1. The crystal structure analysis of the ZnO film was done using a BRUKER D8 EVA software programming. XRD results indicate that the ZnO film has a polycrystalline structure and it grows with a hexagonal wurtzite-type. The main significant peaks for ZnO film were found to be (1 0 0) (0 0 2), (1 0 1), (1 0 2) and (1 1 0). The lattice parameters of the ZnO film were determined by the following relation:

$$\frac{1}{d^2} = \frac{4}{3}\left(\frac{h^2 + hk + k^2}{a^2}\right) + \frac{l^2}{c^2} \quad (1)$$

The lattice parameters were found to be $a = 3.2493 \pm 0.0001$ Å, $c = 5.1968 \pm 0.0001$ Å, $\alpha = \beta = 90^\circ$, $\gamma = 120^\circ$. The obtained lattice constants are in agreement with standard data of Joint Committee on Powder Diffraction Standards (JCPDS) $a = 3.24982$ Å and $c = 5.20661$ Å [23]. The peak broadening with crystallite size and lattice strain due to dislocation can be evaluated by XRD data. The breadth of the Bragg peak is a combination of both instrument and sample dependent effects. In order to dissociate these contributions, we need to collect a diffraction pattern from the line broadening of a standard material such as silicon to determine the instrumental broadening [24]. The instrumental corrected broadening, b_{hkl} corresponding to the diffraction peak of ZnO was estimated by using the relation [25]:

$$\beta_{hkl} = [(\beta_{hkl})^2_{measured} - (\beta^2_{instrumental})]^{1/2}$$

The crystallite size of the ZnO was determined from β_{hkl} of (0 0 2) diffraction peak using Scherrer formula:

$$D = \frac{0.94\lambda}{\beta_{hkl} \cos\theta} \quad (2)$$

where D is the crystallite size, λ is the X-ray wavelength, θ is the Bragg diffraction angle of the (0 0 2) peak. The crystallite size was found to be 34.81 nm. Fig. 2 shows one-dimensional (1D) and three-dimensional (3D) AFM images of the ZnO film. As seen in Fig. 2, the ZnO film is formed from microrings. A single phase of ZnO microrings with outer diameter ranging from 2.2 μm to 1.72 μm and inner diameters ranging from 125 nm to 470 nm was obtained using a Park system XEI analysis software programming.

3.2. Determination of optical band gap of the ZnO film

To determine optical band gap of ZnO film, the reflectance spectra of ZnO film deposited on p-Si wafer was measured. The diffuse reflectance measurements of the ZnO/p-Si sample were carried out using a bare p-Si wafer as a reference. The reflectance (R) spectra of the ZnO film were shown in Fig. 3. As seen in Fig. 3,

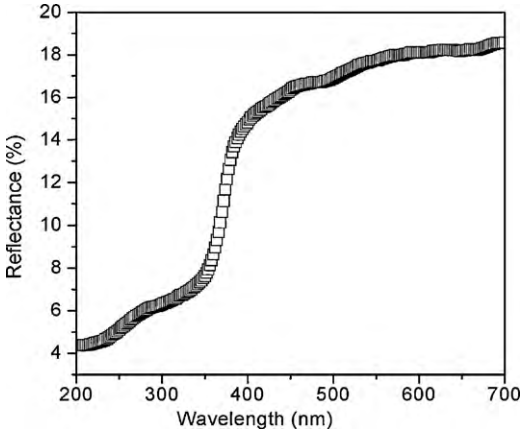

Fig. 3. Reflectance and dR/dλ spectra of the ZnO film.

the reflectance spectra show a strong decrease after 450 nm. This decrease is related to optical transitions occurring in optical band gap. In order to determine the precise value of optical band gap of the ZnO, the reflectance values were converted to absorbance by application of the Kubelka-Munk function [26,27]. The Kubelka-Munk theory is generally used for the analysis of diffuse reflectance spectra obtained from weakly absorbing samples. Kubelka-Munk formula is expressed by the following relation:

$$F(R) = \frac{(1-R)^2}{2R} = \frac{K}{s} \tag{3}$$

where $F(R)$ is the Kubelka-Munk function which corresponds to the absorbance, R is the reflectance, K is the absorption coefficient and s is the scattering coefficient. It is well known that the optical transitions in semiconductor materials are taken place by direct and indirect transitions. The absorption coefficient α for direct transitions is expressed by the following relation [9]:

$$\alpha h\nu = B(h\nu - E_g)^m \tag{4}$$

where α is the linear absorption coefficient of the material, B is an energy-independent constant and E_g is the optical band gap, m is a constant which determines the type of optical transitions and for indirect allowed transition, $m = 2$; and indirect forbidden transition, $m = 3$, for direct allowed transition, $m = 1/2$; for direct forbidden transition, $m = 3/2$. The $F(R)$ values for the ZnO film were obtained using $(1-R)^2/2R$ relation in Eq. (3) [28,29] and Kubelka-Munk function $F(R)$ is directly proportional to the absorbance. Therefore, $F(R)$ values were converted to the linear absorption coefficient by means of $\alpha = F(R)/t = Absorbance/t$ relation [30]; where t is the thickness of the ZnO film. The curve of $(F(R)h\nu/t)^2$ vs. $h\nu$ for the ZnO film was plotted, as shown in Fig. 4. The E_g optical band gap of ZnO film was determined from curve of $(F(R)h\nu/t)^2$ vs. $h\nu$ and was found to be 3.22 eV. The optical band gap of ZnO studied is lower than that of undoped ZnO materials obtained by various methods [31,32]. This suggests that the optical band gap of ZnO semiconductor changes with respect to synthesis method used.

3.3. Current–voltage characteristics of Au/n-ZnO/n-Si Schottky diode

Fig. 5 shows the current–voltage (I–V) characteristics of the Au/n-ZnO/n-Si Schottky diode. As seen in Fig. 5, the diode indicates a rectifying behavior. The ideality factor of the diode was determined from the slope of the linear region of forward bias of Fig. 5 and was found to be 2.01. This shows that the diode exhibits a non-ideal behavior. This behavior of the diode can be analyzed by the

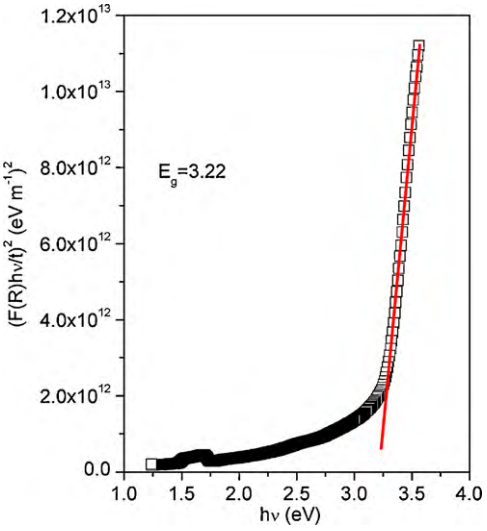

Fig. 4. Plot of $(\alpha h\nu)^2$ vs. ν for the ZnO film.

following relation [33,34]:

$$I = I_o \exp\left(\frac{q(V - IR_s)}{nkT}\right)\left[1 - \exp\left(-\frac{q(V - IR_s)}{kT}\right)\right] \tag{5}$$

where V is the applied voltage, q is the electronic charge, n is the ideality factor, k is the Boltzmann constant, T is the temperature, R_s is the series resistance and I_o is the reverse saturation current. The larger values of n for the studied ZnO diode can be attributed to the presence of interface states, oxide layer on silicon and series resistance and the diode exhibits a non-ideal behavior due to the ideality factor higher than unity and the high value of the ideality factor shows the existence of inhomogeneities of Schottky barrier height. On a semi-log scale and at higher forward bias voltage, the I–V characteristics of the metal–semiconductor contacts deviate considerably from linearity due to the series resistance. Thus, the series resistance effect cannot be ignored. In case of series resistance effect, we can calculate barrier height ϕ_b by modified Norde equations [35]:

$$F(V) = \frac{V_0}{\gamma} - \frac{kT}{q}\ln\left(\frac{I(V)}{A^*AT^2}\right) \tag{6}$$

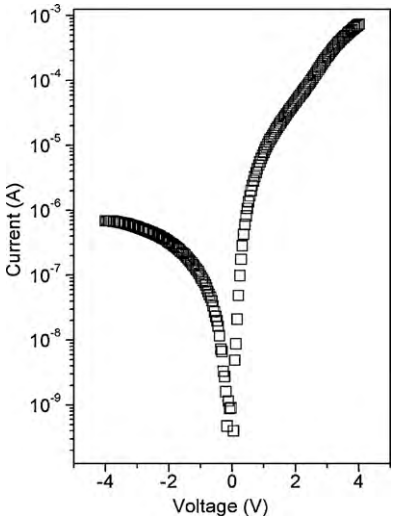

Fig. 5. Current–voltage characteristics of Au/n-ZnO/n-Si Schottky diode.

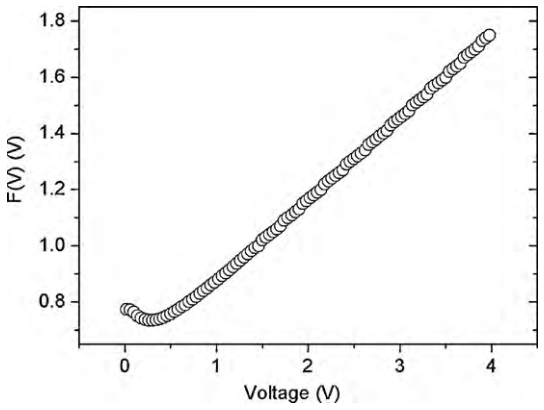

Fig. 6. Norde plot of Au/n-ZnO/n-Si Schottky diode.

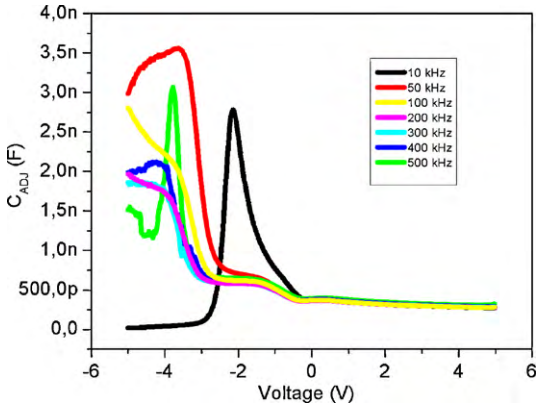

Fig. 8. Corrected capacitance–voltage plots of Au/n-ZnO/n-Si Schottky diode.

and

$$\phi_b = F(V_0) + \frac{V_0}{\gamma} - \frac{kT}{q} \tag{7}$$

where $F(V_0)$ is the minimum value of $F(V)$, and $V_0 = 0.244$ V is the corresponding voltage, $\gamma = 3$ is the integer (dimensionless) greater than n, $I(V)$ is the current obtained from the I–V characteristics, A is the diode contact area, A^* is the Richardson constant ($\sim$36 A cm^{-2} K^{-2} for ZnO) [36]. The Norde plot for the diode was given in Fig. 6. The ϕ_b value of the diode was found to be 0.80 eV. The obtained barrier height of the diode is lower than that of some ZnO Schottky diodes [36,10,37], whereas it is higher than that of Au/ZnO/n-Si/AuSb [14], in which A^* is used as 0.15 A cm^{-2} K^{-2}. Also, the ideality factor of studied Au/n-ZnO/n-Si is higher than those ZnO diodes [36,10,37,14]. This indicates that the rectifying properties of Au/n-ZnO/n-Si change with the structure of ZnO film and interface properties of the diode. Also, these discrepancies in barrier height of the ZnO diodes may be due to the carrier concentration of ZnO films used in diodes.

3.4. Capacitance–voltage and interface state density properties of the Au/n-ZnO/n-Si diode

The C–V and C_{ADJ}–V plots of the Au/n-ZnO/n-Si diode under various frequencies diode are shown in Fig. 7 and Fig. 8. At lower frequencies, the C–V curves show two peaks at negative voltages and then, the peaks were disappeared with increasing frequencies. The presence of the peaks in the C–V plot can be due to the molecular restructuring and reordering of the interface states and series resistance.

At higher frequencies, after certain positive voltage, the capacitance increases and reaches a constant capacitance value at negative voltage. The insulator oxide layer capacitance and series resistance for the diode can be calculated from the admittance behavior. The admittance is defined by the following relation:

$$Z_m = R_s + i\frac{1}{\omega C_{ox}} = G_m + i\omega C_m \tag{8}$$

where R_s is the series resistance and C_{ox} is the capacitance of oxide layer given by [38]

$$C_{ox} = C_m\left(1 + \left(\frac{G_m}{(\omega C_m)}\right)^2\right) \tag{9}$$

where G_m and C_m are the measured conductance and capacitance, respectively, ω is the angular frequency. The corrected capacitance (C_{ADJ}) and corrected conductance (G_{ADJ}) were calculated by the following formulas [38,39]:

$$C_{ADJ} = \frac{(G_m^2 + (\omega C_m)^2)C_m}{a^2 + (\omega C_m)^2} \tag{10}$$

$$G_{ADJ} = \frac{(G_m^2 + (\omega C_m)^2)a}{a^2 + (\omega C_m)^2} \tag{11}$$

with

$$a = G_m - (G_m^2 + (\omega C_m)^2)R_s \tag{12}$$

where G_{ADJ} is series resistance compensated conductance, C_{ADJ} is series resistance compensated parallel model capacitance. The G-V and G_{ADJ}-V plots for the diode were shown in Figs. 9 and 10. As seen in Figs. 9 and 10, the C_{ADJ} and G_{ADJ} plots indicate a peak due the presence of interface states. The peak position of C_{ADJ} and

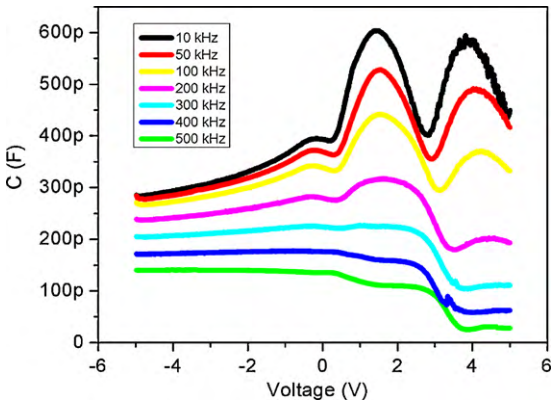

Fig. 7. Capacitance–voltage plots of Au/n-ZnO/n-Si Schottky diode.

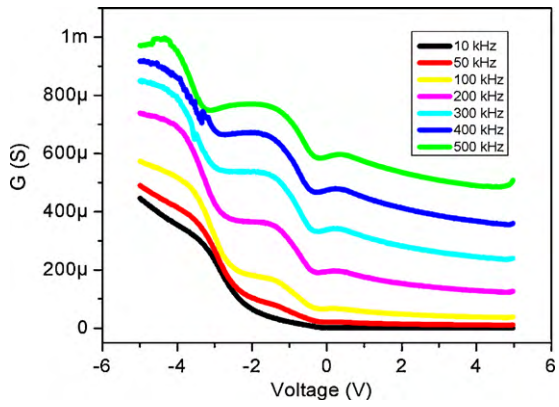

Fig. 9. Conductance–voltage plots of Au/n-ZnO/n-Si Schottky diode.

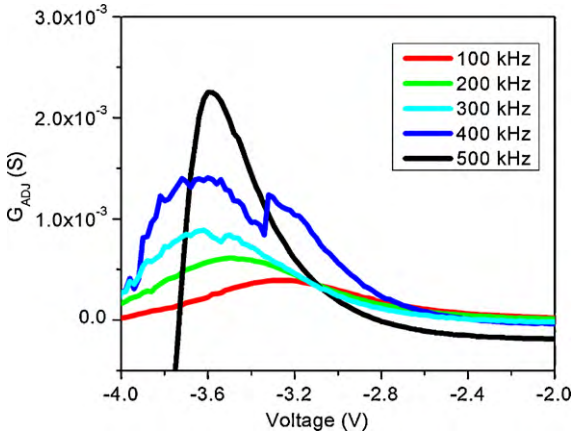

Fig. 10. Corrected conductance–voltage plots of Au/n-ZnO/n-Si Schottky diode.

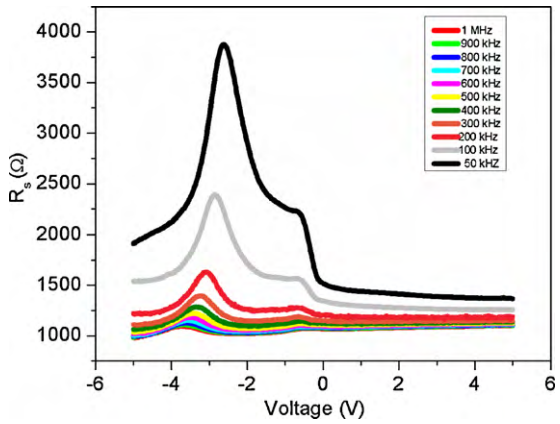

Fig. 11. Series resistance–voltage plots of Au/n-ZnO/n-Si Schottky diode.

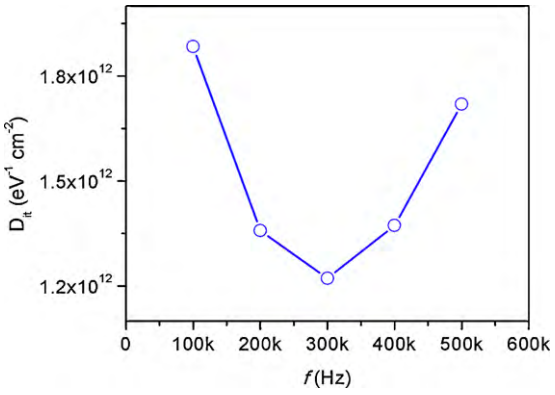

Fig. 12. Interface state density profile of Au/n-ZnO/n-Si Schottky diode.

G_{ADJ} plots shifts towards higher negative voltages with increasing frequency. The peak intensity of G_{ADJ} plots was increased with increasing frequency. This indicates that the interface states can follow the alternating current signal. But at higher frequencies, the peak intensity of G_{ADJ} plots reaches a higher value, suggesting that the interface state charges cannot follow the ac signal. The presence of the peak in the C_{ADJ} and G_{ADJ} of the diode is explained with the interface states and series resistance. The series resistance (R_s) for the diode is calculated from the capacitance and conductance values measured in the accumulation region:

$$R_s = \frac{(G_m/\omega C_m)^2}{1 + (G_m/\omega C_m)^2} G_m \tag{13}$$

The plots of R_s vs. V for the diode are shown in Fig. 11. The obtained R_s values are considerable high and affect the current–voltage characteristics. These high R_s values cause non-ideal behavior resulting from higher ideality factor than unity. The R_s plots indicate a peak and the peak position shifts to higher positive voltage with increase in frequency. The peak height is decreased with increasing frequency, indicating that the interface states change with frequency. The values of series resistance decrease with increasing frequency, because at lower frequencies the interface states can follow the ac signal and yield an excess capacitance, which depend on the frequency [40]. Whereas, at higher frequencies, the R_s values have the lowest values. This occurs because the interface states cannot follow the ac signal and do not make a contribution to interface states. In order to determine the density of interface states (D_{it}) Hill–Coleman method which is a fast and reliable way was used [41]. According to this method, D_{it} can be calculated using the following formula:

$$D_{it} = \frac{2}{qA} \frac{G_{max}/\omega}{[(G_{max}/\omega C_{ox})^2 + (1 - C_m/C_{ox})^2]} \tag{14}$$

where C_m is the measured capacitance, $(G_m/\omega)_{max}$ is the measured conductance, C_{ox} is the capacitance of the insulator layer, A is the area of the diode and ω is the angular frequency. The D_{it} values for the diode were calculated from G_{ADJ} vs. V plots and were shown in Fig. 12. As seen in Fig. 12, the D_{it} value decreases with increasing frequency and then, indicates a minimum and again it increases. This suggests that this change in the interface states may be due to the restructuring and reordering of the interface trapped charges. Also, this behavior indicates the presence of various kinds of interface states with different life times.

The capacitance–voltage characteristics of the Au/n-ZnO/n-Si diode under 500 kHz were shown in Fig. 7. The C–V characteristics of the diode can be analyzed by the following relation [32]:

$$\frac{1}{C^2} = \frac{2(V_{bi} + V)}{A^2 \varepsilon_s q N_d} \tag{15}$$

where V_{bi} is the built-in potential, ε_s is the dielectric constant of ZnO ($\varepsilon_s = 8.5$) [22] and N_d is the donor concentration of ZnO. The N_d and V_{bi} values for the diode were found to be 2.90×10^{15} cm^{-3} and 1.64 V, respectively. The barrier height of the Au/ZnO/n-Si/Ag diode was calculated using following relation [33]:

$$\phi_{b(C-V)} = C_2 V_{bi} + \frac{kT}{q} \ln\left(\frac{N_c}{N_d}\right) \tag{16}$$

where C_2 is a parameter inverse of the ideality factor n ($C_2 = 1/n$), N_c is density of states in the conduction band ($N_c = 3.35 \times 10^{18}$ cm^{-3}) [22] and V_{bi} is the intercept voltage. The barrier height of the diode was calculated using the V_{bi} and N_d values obtained from C^{-2}–V plotted via Eq. (16) and was found to be 0.99 eV. The ϕ_b value obtained from C–V measurement is higher than ϕ_b which is obtained from I–V measurement due to the inhomogeneities such as non-uniformity of the interfacial layer thickness and distributions of the interfacial charges [42,43]. We evaluate that the barrier height is significantly affected by these inhomogeneities. The higher effective barrier heights are related with small and then close to unity ideality factors. This is attributed to the non-uniform interfaces and to lateral inhomogeneities of the barrier heights Schottky diodes [36,44,45].

4. Conclusions

Some physical properties of zinc oxide microrings formed nanoparticles prepared by sol–gel method on n-type silicon

substrate have been investigated. The ZnO film exhibits a polycrystalline grown with a hexagonal wurtzite-type. The optical band gap of the ZnO film was found to be 3.22 eV. The AFM results indicate that the ZnO film is consisted of microrings with nanoparticles. The barrier height ϕ_b and ideality factor n values for the diode were found to be 0.80 eV and 2.01, respectively.

Acknowledgements

This work was partially supported by the National Boron Research Institute (BOREN) (project Number: BOREN-2006-26-Ç25-19). Author wishes to thank BOREN.

References

[1] C. Lin, H. Lin, J. Li, X. Li, J. Alloys Compd. 462 (2008) 175.
[2] C.D. Lokhande, P.M. Gondkar, R.S. Mane, V.R. Shinde, S.-H. Han, J. Alloys Compd. 475 (2009) 304.
[3] Y. Caglar, S. Ilican, M. Caglar, F. Yakuphanoglu, J. Wu, K. Gao, P. Lu, D. Xue, J. Alloys Compd. 481 (2009) 885.
[4] C.E. Benouis, M. Benhaliliba, A. Sanchez Juarez, M.S. Aida, F. Chami, F. Yakuphanoglu, J. Alloys Compd. 490 (2010) 62.
[5] K. Yuan, X. Yin, J. Li, J. Wu, Y. Wang, F. Huang, J. Alloys Compd. 489 (2010) 694.
[6] H.-C. Cheng, C.-F. Chen, C.-Y. Tsay, J.-P. Leu, J. Alloys Compd. 475 (2009) L46.
[7] K.J. Chen, F.Y. Hung, S.J. Chang, S.J. Young, J. Alloys Compd. 479 (2009) 674.
[8] D.C. Look, Mater. Sci. Eng. B 80 (2001) 383.
[9] M. Caglar, S. Ilican, Y. Caglar, F. Yakuphanoglu, Int. J. Mater. Sci. Elect. Res. 1 (2010) 21.
[10] S.J. Young, L.-W. Ji, S.J. Chang, Y.P. Chen, S.-M. Peng, Semicond. Sci. Technol. 23 (2008) 085016.
[11] Z. Ye, G. Yuan, B. Li, L. Zhu, B. Zhao, J. Huang, Mater. Chem. Phys. 93 (2005) 170.
[12] C. Weichsel, O. Pagni, E. vanWyk, A.W.R. Leitch, Superlattice Microst. 39 (2006) 1.
[13] W. Mtangi, F.D. Auret, C. Nyamhere, P.J. JansevanRensburg, M. Diale, A. Chawanda, Physica B 404 (2009) 1092.
[14] Ş. Aydoğan, K. Çınar, H. Asıl, C. Coşkun, A. Türüt, J. Alloys Compd. 476 (2009) 913.
[15] W. Mtangi, F.D. Auret, C. Nyamhere, P.J. JansevanRensburg, A. Chawanda, M. Diale, J.M. Nel, W.E. Meyer, Physica B 404 (2009) 4402.
[16] C. Yan, D. Xue, Adv. Mater. 20 (2008) 1055.
[17] J. Liu, D. Xue, Adv. Mater. 20 (2008) 2622.
[18] J. Yanga, J. Zheng, H. Zhai, X. Yang, L. Yang, Y. Liu, J. Lang, M. Gao, J. Alloys Compd. 489 (2010) 51.
[19] L.H. Van, M.H. Hong, J. Ding, J. Alloys Compd. 449 (2008) 207.
[20] S. Huang, Q. Xiao, H. Zhou, D. Wang, W. Jiang, J. Alloys Compd. 486 (2009) L24.
[21] S.W. Xue, X.T. Zu, W.L. Zhou, H.X. Deng, X. Xiang, L. Zhang, H. Deng, J. Alloys Compd. 448 (2008) 21.
[22] F. Yakuphanoglu, J. Alloys Compd. 494 (2010) 451.
[23] Powder Diffraction File 36-1451 for hexagonal Zinc Oxide, JCPDS-International Center for Diffraction Data, 1997.
[24] J.S. Lee, R.J. De Angelis, Nanostruct. Mater. 7 (1996) 805.
[25] V. Biju, S. Neena, V. Vrinda, S.L. Salini, J. Mater. Sci. 43 (2008) 1175.
[26] A. Escobedo Morales, E. Sanchez Mora, U. Pal, Rev. Mexic. De Fisica S 53 (2007) 18.
[27] V. Senthilkumar, P. Vickraman, R. Ravikumar, J. Sol-Gel. Sci. Technol., doi: 10.1007/s10971-009-2094-z.
[28] M. Caglar, S. Ilican, Y. Caglar, F. Yakuphanoglu, Appl. Surf. Sci. 255 (2009) 4491.
[29] X.-C. Liu, E.-W. Shi, Z.-Z. Chen, H.-W. Zhang, L.-X. Song, H. Wang, S.-D. Yao, J. Cryst. Growth 296 (2006) 135.
[30] R.F. Silva, M.E. Darbello Zaniquelli, J. Non-Cryst. Solids 247 (1999) 248.
[31] A.E. Jimenez-Gonzalez, J.A. Soto Urueta, R. Suarez-Parra, J. Cryst. Growth 192 (1998) 430.
[32] F. Yakuphanoglu, S. Okur, Microelectron. Eng. 87 (2010) 30.
[33] E.H. Rhoderick, R.H. Williams, Metal–Semiconductor Contacts, 2nd ed., Clarendon, Oxford, 1988.
[34] H. Norde, J. Appl. Phys. 50 (1979) 5052.
[35] O. Madelung, M. Schulz, H. Weiss, in: Semimagnetic Semiconductors, Landolt-Bornstein, New, Series, Group III, vol. 17, Part B, Springer, Berlin, 1982.
[36] E. Gür, S. Tüzemen, B. Kılıç, C. Coşkun, J. Phys.: Condens. Matter 19 (2007) 196206.
[37] S. Liang, H. Sheng, Y. Liu, Z. Huo, Y. Lu, H. Shen, J. Cryst. Growth 225 (2001) 110.
[38] E.H. Nicollian, A. Goetzberger, Bell Syst. Technol. J. 46 (1967) 1055.
[39] I. Dökme, Ş. Altındal, T. Tunç, I. Uslu, Microelectron. Reliab. 50 (2010) 39.
[40] Ş. Karataş, A. Türüt, Vacuum 74 (2004) 45.
[41] W.A. Hill, C.C. Coleman, Solid State Electron. 23 (1980) 987.
[42] Y.P. Song, R.L. Van Meirhaeghe, W.H. Laflere, F. Cardon, Solid State Electron. 29 (6) (1986) 633.
[43] F. Yakuphanoglu, B.F. Şenkal, J. Phys. Chem. C 111 (2007) 1840.
[44] R.F. Schmitsdorf, T.U. Kampen, W. Mönch, J. Vac. Sci. Technol. B 15 (4) (1997) 1221.
[45] W.P. Leroy, K. Opsomer, S. Forment, R.L. Van Meirhaeghe, Solid State Electron. 49 (2005) 878.